





## Single-particle momentum distribution of Efimov states in noninteger dimensions

D. S. Rosa <sup>1</sup>, T. Frederico <sup>1</sup>, G. Krein <sup>2</sup>, and M. T. Yamashita <sup>2</sup>

<sup>1</sup>*Instituto Tecnológico de Aeronáutica, DCTA, 12228-900 São José dos Campos, São Paulo, Brazil*

<sup>2</sup>*Instituto de Física Teórica, Universidade Estadual Paulista,  
Rua Dr. Bento Teobaldo Ferraz, 271-Bloco II, 01140-070 São Paulo, São Paulo, Brazil*



(Received 30 May 2023; accepted 25 August 2023; published 7 September 2023)

We studied the single-particle momentum distribution of mass-imbalanced Efimov states embedded in noninteger dimensions. The contact parameters, which can be related to the thermodynamic properties of the gas, were extracted from the tail of the single-particle momentum densities. We studied the dependence of the contact parameters on the progressive change in the noninteger dimension, ranging from three ( $D = 3$ ) to two ( $D = 2$ ) dimensions. Within this interval, we move from the  $D = 3$  regime where the Efimov discrete-scale symmetry drives the physics to close to the critical dimension, which depends on the mass imbalance, where the continuum-scale symmetry takes place. We found that the two- and three-body contacts grow significantly in magnitude with the decrease of the noninteger dimension towards the critical dimension, impacting observables of resonantly interacting trapped Bose gases.

DOI: [10.1103/PhysRevA.108.033307](https://doi.org/10.1103/PhysRevA.108.033307)

### I. INTRODUCTION

More than 20 years of advances in cold-atom technologies not only allowed experimental confirmation of Efimov states in homonuclear [1–3] and heteronuclear atomic systems [4–6] but also led to the explosion of the rich research area of Efimov physics. Nowadays, atomic traps provide remarkable freedom to conveniently manipulate energies and geometries to study several aspects of few-body physics. Magnetic fields tuned to a Feshbach resonance [7] allow controlling the value of scattering lengths, and asymmetrical magnetic fields allow squeezing atomic clouds to create three- [8], two- [9], and one-dimensional [10] environments.

The achievement of the universal regime, in that the scattering length tends to infinity, effectively made possible the experimental confirmation of Efimov states—weakly bound systems originally predicted by Efimov in 1970 when he was studying three identical bosons [11,12]. This effect is characterized by a three-boson system exhibiting an infinite number of geometrically spaced energy levels (see Refs. [13–16] for reviews) and was first observed through indirect measurement of the three-body loss peaks in trapped cold atomic systems [17]. Nowadays, advanced experimental techniques allow direct measurement of the binding energies of two- and three-body molecules in cold atomic gases [18,19].

A myriad of developments followed the experimental confirmation of Efimov states. One of the most notable developments is the measurements in cold gases (e.g., those in Refs. [20–24]) of the contacts introduced by Tan [25–27], which are remarkable universal quantities that parametrize thermodynamic relations between macroscopic observables such as the momentum distribution, energy, and response functions of low-temperature gases interacting via short-range interactions. Tan found those universal relations by studying the tail of the single-particle momentum distribution for a two-component Fermi gas in the presence of strong interactions. For unitary Bose gases, there is one more contact parameter

[28–31] related to the probability of finding three atoms close together.

For a long time, the determinant role played by the spatial dimension in the presence of the Efimov effect in a three-body system has been known—it is present in three dimensions but absent in two [32,33]. As a consequence, in two dimensions physical properties of few- and many-boson systems scale with the two-body energies in the limit of zero-range interactions [34]. The contacts in particular also reflect such a scaling [35]. Therefore, the sequential disappearance of the most excited bound states during a progressive change in the effective dimension of a confined resonant three-body system should also have consequences for the contacts extracted from the tail of the single-boson momentum distributions.

An efficient way to study a dimensional crossover is to introduce a continuous dimension  $D$  and solve the three-body problem employing only the interatomic interactions, with the  $D$ -dependent centrifugal barrier mocking the external squeezing potential [36–40]. Although technically convenient to implement, connecting  $D$  to an experimental setup is a key issue. For three identical bosons in a deformed trap induced by an external harmonic potential, such a connection was suggested in Ref. [41] to be

$$\frac{3(D-2)}{(3-D)(D-1)} = \left( \frac{b_{ho}}{r_{2D}} \right)^2, \quad (1.1)$$

where  $b_{ho}$  is the oscillator length and  $r_{2D}$  is the root-mean-square radius of the bound three-body system in two dimensions. A similar expression for a two-body system was suggested in Ref. [36].

Despite the advances that led to the possibility of compressing and expanding atomic clouds, effectively creating two- [9] and one-dimensional [10] setups, to the best of our knowledge, there have not been any experiments designed to study the effects of continuous deformation of the trap on Efimov physics. While awaiting such an experimental

possibility, the rich physics revealed by previous theoretical studies warrants exploring this subject in connection with the contacts. Within such a perspective, we study in this work the  $D$  dependence of the two- and three-body contact parameters in mass-imbalanced three-body systems featuring the Efimov effect. We extract the contact parameters from the single-particle momentum distributions at high momentum values. We treat the three-body problem in terms of  $D$ -dimensional hyperspherical coordinates [42] and solve the problem analytically using the Bethe-Peierls (BP) boundary conditions employing the method we introduced in Ref. [43].

This work is organized as follows. In Sec. II, for a system composed of two  $A$  atoms and a third one,  $B$ , we review the derivation of the analytical  $D$ -dimensional Faddeev components of the mass-imbalanced three-body bound-state wave function. Section III is devoted to the derivation of the momentum distribution of particle  $B$  in  $D$  dimensions. We also discuss in this section the high-momentum regime of the single-particle momentum distribution from which the two- and three-body contacts are obtained. Section IV shows quantitative results for the momentum density and relates them to the two- and three-body contacts for three identical bosons and a mass-imbalanced system of the form  ${}^6\text{Li}$ - ${}^{133}\text{Cs}_2$ . The conclusions are given in Sec. V. Appendixes A to D give the details of the large-momentum subleading contributions to the single-particle momentum distribution discussed in Sec. III. In Appendix E, we display the numerical values of the two- and three-body parameters for different mass configurations in three dimensions.

## II. $D$ -DIMENSIONAL EFIMOV STATE

In this section, we review the derivation of the  $D$ -dimensional three-body wave function of an Efimov state for a mass-imbalanced system at unitarity, according to our approach introduced in Ref. [43]. We found the solution of the energy eigenvalue equation for a three-particle system interacting with a zero-range potential by considering the Bethe-Peierls boundary condition [44] on the free-energy eigenstate. This method uses the fact that the short-range region, where the interaction strongly affects the wave function, can be neglected because only the asymptotic region, parametrized by the scattering length, is relevant.

### A. Configuration space

We consider three different particles with masses  $m_i$ ,  $m_j$ , and  $m_k$  and coordinates  $\mathbf{x}_i$ ,  $\mathbf{x}_j$ , and  $\mathbf{x}_k$ . One can eliminate the center-of-mass coordinate and describe the system in terms of two relative Jacobi coordinates. The three sets of such coordinates are given by

$$\mathbf{r}_i = \mathbf{x}_j - \mathbf{x}_k, \quad \boldsymbol{\rho}_i = \mathbf{x}_i - \frac{m_j \mathbf{x}_j + m_k \mathbf{x}_k}{m_j + m_k}, \quad (2.1)$$

where  $(i, j, k)$  are taken cyclically among  $(1, 2, 3)$ . The Faddeev decomposition of the three-body wave function allows us to write it as a sum of three components. In the center of mass, it reads

$$\Psi(\mathbf{x}_1, \mathbf{x}_2, \mathbf{x}_3) = \psi^{(1)}(\mathbf{r}_1, \boldsymbol{\rho}_1) + \psi^{(2)}(\mathbf{r}_2, \boldsymbol{\rho}_2) + \psi^{(3)}(\mathbf{r}_3, \boldsymbol{\rho}_3).$$

Each Faddeev component satisfies the free Schrödinger eigenvalue equation:

$$\left[ \frac{1}{2\eta_i} \nabla_{\mathbf{r}_i}^2 + \frac{1}{2\mu_i} \nabla_{\boldsymbol{\rho}_i}^2 - E_3 \right] \psi^{(i)}(\mathbf{r}_i, \boldsymbol{\rho}_i) = 0, \quad (2.2)$$

where  $E_3$  is the energy eigenvalue. The reduced masses are given by  $\eta_i = m_j m_k / (m_j + m_k)$  and  $\mu_i = m_i (m_j + m_k) / (m_i + m_j + m_k)$ . The BP boundary condition applies to the total wave function; when applied to the chosen coordinates pair  $(\mathbf{r}_i, \boldsymbol{\rho}_i)$ , it reads, in the unitary limit  $a \rightarrow \infty$ ,

$$\left[ \frac{\partial}{\partial r_i} r_i^{\frac{D-1}{2}} \Psi(\mathbf{r}_i, \boldsymbol{\rho}_i) \right]_{r_i \rightarrow 0} = \frac{3-D}{2} \left[ \frac{\Psi(\mathbf{r}_i, \boldsymbol{\rho}_i)}{r_i^{\frac{3-D}{2}}} \right]_{r_i \rightarrow 0}. \quad (2.3)$$

This solution strategy was applied to different particles and spins in Ref. [45], and we adapted it to  $D$  dimensions closely following Efimov's original derivation [46].

For convenience, we simplify the form of the kinetic energies, introducing the new coordinates  $\mathbf{r}'_i = \sqrt{\eta_i} \mathbf{r}_i$  and  $\boldsymbol{\rho}'_i = \sqrt{\mu_i} \boldsymbol{\rho}_i$ . The three sets of primed coordinates are related to each other by the orthogonal transformations

$$\begin{aligned} \mathbf{r}'_j &= -\mathbf{r}'_k \cos \theta_i + \boldsymbol{\rho}'_k \sin \theta_i, \\ \boldsymbol{\rho}'_j &= -\mathbf{r}'_k \sin \theta_i - \boldsymbol{\rho}'_k \cos \theta_i, \end{aligned} \quad (2.4)$$

where  $\tan \theta_i = [m_i M / (m_j m_k)]^{1/2}$ , with  $M = m_1 + m_2 + m_3$ .

Considering three distinct bosons in a state with vanishing total angular momentum, we can write a reduced Faddeev component as  $\chi_0^{(i)}(r'_i, \rho'_i) = (r'_i \rho'_i)^{(D-1)/2} \psi^{(i)}(r'_i, \rho'_i)$ . The solution of the corresponding eigenvalue equation for  $\chi_0^{(i)}$  is found by using hyperspherical coordinates to separate the variables  $r'_i = R \sin \alpha_i$  and  $\rho'_i = R \cos \alpha_i$ , so that we can write  $\chi_0^{(i)}(R, \alpha_i) = C^{(i)} F(R) G^{(i)}(\alpha_i)$ , where  $R^2 = r_i'^2 + \rho_i'^2$ ,  $\alpha_i = \arctan(r'_i / \rho'_i)$ , and the coefficients  $C^{(i)}$  give the weight between the different Faddeev components for mass-imbalanced systems. The functions  $F(R)$  and  $G^{(i)}(\alpha_i)$  satisfy the following differential equations:

$$\left[ -\frac{\partial^2}{\partial R^2} + \frac{s_n^2 - 1/4}{R^2} + 2\kappa_0^2 \right] \sqrt{R} F(R) = 0, \quad (2.5)$$

$$\left[ -\frac{\partial^2}{\partial \alpha_i^2} - s_n^2 + \frac{(D-1)(D-3)}{\sin^2 2\alpha_i} \right] G^{(i)}(\alpha_i) = 0, \quad (2.6)$$

where  $-\kappa_0^2 = E_3$  and  $s_n$  is recognized as the Efimov parameter.

Equation (2.6) can be solved in two steps. First, we change the variable  $z_i = \cos 2\alpha_i$  to write Eq. (2.6) as

$$\begin{aligned} 4(1-z_i^2) \frac{\partial^2 G^{(i)}(z_i)}{\partial z_i^2} - 4z_i \frac{\partial G^{(i)}(z_i)}{\partial z_i} \\ + \left[ s_n^2 - \frac{(D-1)(D-3)}{1-z_i^2} \right] G^{(i)}(z_i) = 0. \end{aligned} \quad (2.7)$$

Next, to arrive at the desired equation we define  $G^{(i)}(z_i) = (1-z_i^2)^{1/4} g^{(i)}(z_i)$ , so that Eq. (2.7) becomes the associated

Legendre differential equation [47]

$$(1 - z_i^2) \frac{\partial^2 g^{(i)}(z_i)}{\partial z_i^2} - 2z_i \frac{\partial g^{(i)}(z_i)}{\partial z_i} + \left[ \frac{s_n^2 - 1}{4} - \frac{(D-2)^2/4}{1 - z_i^2} \right] g^{(i)}(z_i) = 0, \quad (2.8)$$

with known analytical solutions:

$$G^{(i)}(\alpha_i) = \sqrt{\sin 2\alpha_i} \left\{ P_{s_n/2-1/2}^{D/2-1}(\cos 2\alpha_i) - \frac{2}{\pi} \tan[\pi(s_n - 1)/2] Q_{s_n/2-1/2}^{D/2-1}(\cos 2\alpha_i) \right\}, \quad (2.9)$$

where  $P_n^m(x)$  and  $Q_n^m(x)$  are the associated Legendre functions. A finite value for the Faddeev component  $\psi^{(i)}$  at  $\rho_i = 0$  imposes  $G^{(i)}(\alpha_i = \pi/2) = 0$  since  $\rho_i' = R \cos \alpha_i$ .

Considering the solution of the hyperradial equation (2.5) and the hyperangular eigenfunction, Eq. (2.9), each Faddeev component of the wave function is written as [43]

$$\begin{aligned} \psi^{(i)}(r_i', \rho_i') &= C^{(i)} \frac{K_{s_n}(\sqrt{2}\kappa_0 \sqrt{r_i'^2 + \rho_i'^2})}{(r_i'^2 + \rho_i'^2)^{D/2-1/2}} \frac{\sqrt{\sin[2 \arctan(r_i'/\rho_i')]} }{\{\cos[\arctan(r_i'/\rho_i')] \sin[\arctan(r_i'/\rho_i')]\}^{D/2-1/2}} \\ &\times \left[ P_{s_n/2-1/2}^{D/2-1} \{\cos[2 \arctan(r_i'/\rho_i')]\} - \frac{2}{\pi} \tan[\pi(s_n - 1)/2] Q_{s_n/2-1/2}^{D/2-1} \{\cos[2 \arctan(r_i'/\rho_i')]\} \right], \end{aligned} \quad (2.10)$$

where  $K_{s_n}$  is the modified Bessel function of the second kind.

The BP boundary condition at the unitary limit [43] must be satisfied by the three-body wave function, written as the sum of its Faddeev components given in Eq. (2.10), when each relative distance between two of the particles tends to zero. Taking the three cyclic permutations of  $\{i, j, k\}$ , we have a homogeneous linear system,

$$\begin{aligned} \frac{C^{(i)}}{2} \left[ (\cot \alpha_i)^{\frac{D-1}{2}} \left( \sin 2\alpha_i \frac{\partial}{\partial \alpha_i} + D - 3 \right) G^{(i)}(\alpha_i) \right]_{\alpha_i \rightarrow 0} \\ + (D-2) \left[ \frac{C^{(j)} G^{(j)}(\theta_k)}{(\sin \theta_k \cos \theta_k)^{\frac{D-1}{2}}} + \frac{C^{(k)} G^{(k)}(\theta_j)}{(\sin \theta_j \cos \theta_j)^{\frac{D-1}{2}}} \right] = 0, \end{aligned} \quad (2.11)$$

and using  $i \neq j \neq k$ , we can explicitly write the set of three linear equations for an  $ABC$  system.

The Efimov parameter  $s_n$  is then computed by solving the characteristic equation for the linear set obtained from Eq. (2.11), which reduces to one and two equations for  $AAA$  and  $AAB$  systems, respectively. When  $s_n$  is purely imaginary ( $s_n \rightarrow is_0$ ), the effective  $1/R^2$  potential in Eq. (2.5) is attractive, giving rise to the discrete scaling symmetry and to the well-known Landau “fall to the center,” where the energy spectrum is unbounded from below, namely, the collapse of the three-body system discovered by Thomas [48] long ago. In particular, for the  $AAA$  system in  $D = 3$  the characteristic equation for  $s_0$  reduces to the standard Efimov equation.

## B. Momentum space

To obtain the single-particle momentum distributions, we need to perform the Fourier transform (FT) of the Faddeev wave functions, Eq. (2.10). However, instead of performing the FT directly, we first obtain the spectator amplitude, closely following Ref.'s [29] derivation for three identical bosons for  $D = 3$ . The asymptotic form of the associated Legendre poly-

nomials for  $r_i' \rightarrow 0$  in the hyperangular part of the Faddeev wave function, Eq. (2.9), has to be used, which leads to

$$\begin{aligned} \psi^{(i)}(\rho_i', r_i') &\underset{r_i' \rightarrow 0}{=} C^{(i)} \frac{\sqrt{2}[1 - i \cot(D\pi/2) \tanh(s_0\pi/2)]}{\Gamma(2 - D/2)} \\ &\times r_i'^{2-D} \frac{K_{is_0}(\sqrt{2}\kappa_0 \rho_i')}{\rho_i'}, \end{aligned} \quad (2.12)$$

where  $\Gamma(z)$  is the gamma function defined for all complex numbers  $z$ , except for the nonpositive integers—this condition restricts the validity of our results to the interval  $2 \leq D < 4$ .

The spectator function, namely,  $B^{(i)}(\rho_i)$ , can be found by taking advantage of the fact that each Faddeev component  $\psi^{(i)}(\rho_i', r_i')$  obeys Schrödinger's equation for the contact interaction, written as

$$[\nabla_{r_i'}^2 + \nabla_{\rho_i'}^2 - 2\kappa_0^2] \psi^{(i)}(r_i', \rho_i') = \delta(r_i') B^{(i)}(\rho_i'). \quad (2.13)$$

We substitute Eq. (2.12) in (2.13), which, in the limit  $r_i' \rightarrow 0$ , gives

$$\begin{aligned} B^{(i)}(\rho_i') &= C^{(i)} \frac{2^{3/2} \pi^{D/2} [1 - i \cot(D\pi/2) \tanh(s_0\pi/2)]}{\Gamma(D/2) \Gamma(2 - D/2)} \\ &\times \frac{K_{is_0}(\sqrt{2}\kappa_0 \rho_i')}{\rho_i'}. \end{aligned} \quad (2.14)$$

Now, we take the  $D$ -dimensional FT

$$\int d^D \rho_i' \exp(-i\mathbf{q}_i' \cdot \boldsymbol{\rho}_i') B^{(i)}(\rho_i') = \chi^{(i)}(q_i') \quad (2.15)$$

to write the spectator function in momentum space ( $q_i' = q_i/\sqrt{\mu_i}$ ) as

$$\begin{aligned} \chi^{(i)}(q_i') &= C^{(i)} \mathfrak{F}_{(D,s_0)} \kappa_0^{1-D} \\ &\times H_2 \tilde{F}_1 \left( \mathcal{F}_{(D,s_0)}^*, \mathcal{F}_{(D,s_0)}, \frac{D}{2}, -\frac{q_i'^2}{2\kappa_0^2} \right), \end{aligned} \quad (2.16)$$

where

$$\begin{aligned} \tilde{\mathfrak{F}}_{(D,s_0)} \equiv & i \frac{2^{D/2+1} \pi^{D-1} \Gamma[\mathcal{F}_{(D,s_0)}] \Gamma[\mathcal{F}_{(D,s_0)}^*]}{(D-2)} \\ & \times \cos\left(\frac{\pi}{2}(D - is_0)\right) \operatorname{csch}\left(\frac{\pi}{2}s_0\right) \end{aligned} \quad (2.17)$$

and  $H_2\tilde{F}_1(a, b, c, z)$  is the regularized hypergeometrical function with  $\mathcal{F}_{(D,s_0)} \equiv (D-1 + is_0)/2$ . The characteristic log-periodic behavior of the spectator functions exhibited in the asymptotic form of the spectator functions for the range of noninteger dimensions where the Efimov effect exists is found from Eq. (2.16) at large momentum as

$$\begin{aligned} \chi_0^{(i)}(q_i) = & C^{(i)} \tilde{\mathfrak{F}}_{(D,s_0)} 2\sqrt{\operatorname{Re}(\mathcal{G})^2 + \operatorname{Im}(\mathcal{G})^2} \\ & \times \left(\frac{q_i}{\sqrt{2}}\right)^{1-D} \cos\left[s_0 \ln\left(\frac{q_i}{\sqrt{2}\kappa_0^*}\right)\right], \end{aligned} \quad (2.18)$$

where  $\kappa_0^* \equiv \kappa_0 / \exp[\arctan[\operatorname{Im}(\mathcal{G})/\operatorname{Re}(\mathcal{G})]/s_0]$  and

$$\mathcal{G} = \frac{\Gamma(\mathcal{F}_{(D,s_0)} - \mathcal{F}_{(D,s_0)}^*)}{\Gamma(\mathcal{F}_{(D,s_0)} - D/2 - 1)\Gamma(\mathcal{F}_{(D,s_0)})}. \quad (2.19)$$

We note that the asymptotic form of the spectator function in Eq. (2.18) also corresponds to the limit of vanishing three-body energy, with  $\kappa_0^*$  associated with the necessary three-body scale parameter, which is chosen to match Eq. (2.18) with the large-momentum behavior of Eq. (2.16) for the finite-energy spectator function. The normalization constants are solutions of Eq. (2.11), namely, the linear homogeneous system that determines the Efimov parameter.

Figure 1 shows the spectator functions, Eq. (2.16), compared to the zero-energy case, Eq. (2.18), conveniently normalized to one for an  $AAB$  system with  $A = {}^{133}\text{Cs}$  and  $B = {}^6\text{Li}$  embedded in two different dimensions, namely,  $D = 3$  (top panel) and  $2.5$  (bottom panel). In the low-momentum region, the damping of the spectator amplitude with respect to the zero-energy case is an effect of the finite three-body binding energy. The impact of changing the dimension in which the  ${}^6\text{Li}$ - ${}^{133}\text{Cs}_2$  system is embedded is manifested mainly in the different log periodicities of the spectator functions. The period increases to infinity as the system approaches the critical dimension,  $D = 2.231$ , for which the Efimov state disappears. The increasing separation of the log-periodic nodes towards the critical dimension is illustrated by comparing the top and bottom panels of Fig. 1, where the  ${}^6\text{Li}$ - ${}^{133}\text{Cs}_2$  system is forced to decrease from 3 to 2.5 dimensions, respectively. We reproduce analytically the numerical results obtained in Ref. [49] for  $D = 3$ .

### III. MOMENTUM DISTRIBUTION

In this section, we compute the momentum distribution of particle  $B$  for  $AAB$  systems at the unitary limit in  $D$  dimensions. We recall that particle  $B$  is the one responsible for giving rise to an effective Efimov-like potential in the limit of heavy  $A$ , as we showed in Ref. [39]. We recall that in three dimensions, Ref. [29] computed the momentum density for three identical bosons, and Ref. [49] obtained the momentum densities for an  $AAB$  system.

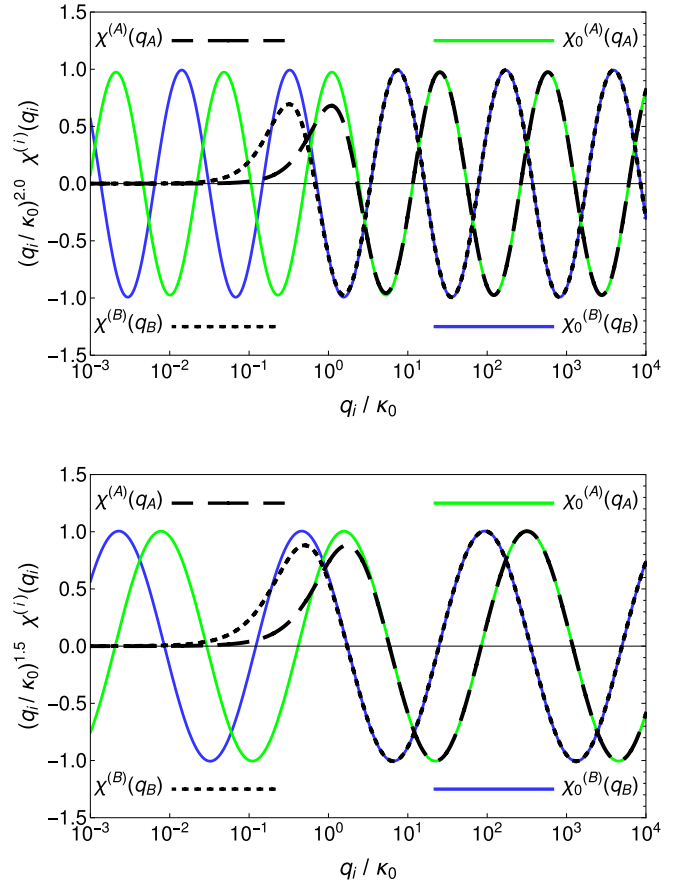


FIG. 1. Spectator functions in momentum space for the  ${}^6\text{Li}$ - ${}^{133}\text{Cs}_2$  system with finite three-body energy  $\chi^{(i)}(q_i)$  ( $i = A \equiv {}^{133}\text{Cs}$  or  $B \equiv {}^6\text{Li}$ ), computed with Eq. (2.16) for  $\chi^{(A)}(q_A)$  (long-dashed line) and  $\chi^{(B)}(q_B)$  (short-dashed line), compared to the zero-energy case from Eq. (2.18) for  $\chi_0^{(A)}(q_A)$  (green solid line) and  $\chi_0^{(B)}(q_B)$  (blue solid line). Top: three dimensions. Bottom:  $D = 2.5$ , which corresponds to a harmonic-trap length of  $b_{ho}/r_{2D} = \sqrt{2}$ .

We start by defining  $\mathbf{k}_\alpha$  ( $\alpha = i, j, k$ ) as the momenta of each particle in the rest frame. We have that the Jacobi momenta from one particle to the center of mass of the other two and the relative momentum of the pairs are given, respectively, by

$$\mathbf{q}_i = \mu_i \left( \frac{\mathbf{k}_i}{m_i} - \frac{\mathbf{k}_k + \mathbf{k}_k}{m_j + m_k} \right), \quad \mathbf{p}_i = \eta_i \left( \frac{\mathbf{k}_j}{m_j} - \frac{\mathbf{k}_k}{m_k} \right). \quad (3.1)$$

In the following, we define the single-particle momentum distribution for particles of types  $A$  and  $B$ . The Faddeev components of the three-body wave function for a zero-range interacting system, composed of two  $A$  identical particles and a third one,  $B$ , can be written using the FT of Eq. (2.13) and the spectator function given by Eq. (2.16).

We start writing the  $AAB$  bound-state wave function in the basis  $|\mathbf{q}_B \mathbf{p}_B\rangle$ ,

$$\begin{aligned} \langle \mathbf{q}_B \mathbf{p}_B | \Psi \rangle = & \frac{1}{E_3 + p_B^2/2\eta_B + q_B^2/2\mu_B} \left[ \chi^{(B)}(\mathbf{q}_B) \right. \\ & \left. + \chi^{(A)}\left(\left|\mathbf{p}_B - \frac{\mathbf{q}_B}{2}\right|\right) + \chi^{(A)}\left(\left|\mathbf{p}_B + \frac{\mathbf{q}_B}{2}\right|\right) \right], \end{aligned} \quad (3.2)$$

and in the basis  $|\mathbf{q}_A \mathbf{p}_A\rangle$ ,

$$\begin{aligned} \langle \mathbf{q}_A \mathbf{p}_A | \Psi \rangle &= \frac{1}{E_3 + p_A^2/2\eta_A + q_A^2/2\mu_A} \\ &\times \left[ \chi^{(A)}(\mathbf{q}_A) + \chi^{(B)} \left( \left| \mathbf{p}_A - \frac{\mathbf{q}_A}{1 + \mathcal{A}^{-1}} \right| \right) \right. \\ &\left. + \chi^{(A)} \left( \left| \mathbf{p}_A + \frac{\mathbf{q}_A}{1 + \mathcal{A}} \right| \right) \right]. \end{aligned} \quad (3.3)$$

Here, we use  $m_A = 1$  in the mass ratio  $\mathcal{A} = m_B/m_A$ .

The momentum distributions in  $D$  dimensions for particles  $A$  and  $B$  are given, respectively, by

$$n_A(q_A) = \int d^D p_A |\langle \mathbf{q}_A \mathbf{p}_A | \Psi \rangle|^2, \quad (3.4)$$

$$n_B(q_B) = \int d^D p_B |\langle \mathbf{q}_B \mathbf{p}_B | \Psi \rangle|^2. \quad (3.5)$$

The  $AAB$  wave function can be determined, up to an overall constant, by obtaining the coefficients of the spectator functions from the solution of the homogeneous linear system (2.11). We use the following normalization condition:

$$\int d^D q_B n_B(q_B) = 1 \text{ or } \int d^D q_A n_A(q_A) = 1. \quad (3.6)$$

From Eqs. (3.2) and (3.5), we can split the momentum density into nine terms, which can be reduced to four, considering the symmetry between the two identical  $A$  particles. This simplifies the computation of the momentum density to four contributions:

$$n_B(q_B) = n_1(q_B) + n_2(q_B) + n_3(q_B) + n_4(q_B), \quad (3.7)$$

which are given by

$$n_1(q_B) = |\chi^{(B)}(q_B)|^2 \int d^D p_B \frac{1}{(E_3 + p_B^2 + q_B^2 \frac{\mathcal{A}+2}{4\mathcal{A}})^2}, \quad (3.8)$$

$$n_2(q_B) = 2 \int d^D p_B \frac{|\chi^{(A)}(|\mathbf{p}_B - \mathbf{q}_B/2|)|^2}{(E_3 + p_B^2 + q_B^2 \frac{\mathcal{A}+2}{4\mathcal{A}})^2}, \quad (3.9)$$

$$\begin{aligned} n_3(q_B) &= 2\chi^{(B)*}(q_B) \int d^D p_B \frac{\chi^{(A)}(|\mathbf{p}_B - \mathbf{q}_B/2|)}{(E_3 + p_B^2 + q_B^2 \frac{\mathcal{A}+2}{4\mathcal{A}})^2}, \\ &+ \text{c.c.}, \end{aligned} \quad (3.10)$$

$$n_4(q_B) = \int d^D p_B \frac{\chi^{(A)*}(|\mathbf{p}_B - \mathbf{q}_B/2|)\chi^{(A)}(|\mathbf{p}_B + \mathbf{q}_B/2|)}{(E_3 + p_B^2 + q_B^2 \frac{\mathcal{A}+2}{4\mathcal{A}})^2} + \text{c.c.} \quad (3.11)$$

Our task now is to evaluate the integral expressions in Eqs. (3.8)–(3.11) and extract the contacts from the large-momentum tail of the distribution densities. The contribution  $n_1(q_B)$  is straightforward to calculate:

$$\begin{aligned} n_1(q_B) &= \frac{|\chi^{(B)}(q_B)|^2}{q_B^{4-D}} S_D \frac{\pi}{4} \csc\left(\frac{D\pi}{2}\right) (2-D) \\ &\times \left(\frac{\mathcal{A}+2}{4\mathcal{A}}\right)^{D/2-2}, \end{aligned} \quad (3.12)$$

where  $S_D$  is the area of a  $D$ -dimensional sphere. The second contribution,  $n_2(q_B)$ , can be computed from Eq. (3.9) making the change in variables  $\mathbf{p}_B - \mathbf{q}_B/2 = \mathbf{q}_A$  as

$$n_2(q_B) = 2 \int d^D q_A \frac{|\chi^{(A)}(q_A)|^2}{(q_A^2 + \mathbf{q}_A \cdot \mathbf{q}_B + q_B^2 \frac{\mathcal{A}+1}{2\mathcal{A}})^2}. \quad (3.13)$$

In order to identify the leading-order term in the large-momentum region, we perform the manipulation

$$\begin{aligned} n_2(q_B) &= 2 \int d^D q_A |\chi^{(A)}(q_A)|^2 \\ &\times \left[ \frac{1}{(q_A^2 + \mathbf{q}_A \cdot \mathbf{q}_B + q_B^2 \frac{\mathcal{A}+1}{2\mathcal{A}})^2} - \frac{4\mathcal{A}^2}{(\mathcal{A}+1)^2} \frac{1}{q_B^4} \right] \\ &+ \frac{C_2}{q_B^4}, \end{aligned} \quad (3.14)$$

where  $C_2$  is the two-body contact, given by

$$C_2 = \frac{8\mathcal{A}^2}{(\mathcal{A}+1)^2} S_D \int_0^\infty dq_A q_A^{D-1} |\chi^{(A)}(q_A)|^2. \quad (3.15)$$

The contact  $C_2$  can be related to the derivative with respect to the scattering length of the gas's mean energy (or mean free energy at nonzero temperature). It has the dimension  $(\text{length})^{D-4}$  and therefore scales as  $C_2 \propto \kappa_0^{4-D}$ . We observe that for  $D = 3$  Ref. [50] presented a general virial theorem for a Hamiltonian with an arbitrary domain. There were derived virial theorems for several systems; one of them is an Efimov state with zero-range interaction and arbitrary scattering length. In principle, the Efimov effect in noninteger dimensions does not bring any additional new length scales to the problem; as such, we assumed that similar relations are also valid in these situations.

From the integral representations in Eqs. (3.8)–(3.11), we obtain the oscillatory and nonoscillatory contributions of each of the four components of the momentum density at large momentum (detailed calculations of the subleading contributions for  $n_1$  to  $n_4$  at large momentum can be found in Appendixes A to D). The leading and subleading contributions in the asymptotic region are given by

$$\begin{aligned} n_B(q_B) &= \frac{C_2}{q_B^4} + \frac{C'_3}{q_B^{D+2}} + \frac{C_3}{q_B^{D+2}} \\ &\times \cos \left[ 2s_0 \ln \left( \frac{q_B/\kappa_0^*}{(4\mu_A\mu_B)^{1/4}} \right) + \Phi \right] + \dots, \end{aligned} \quad (3.16)$$

where  $C'_3$  leads to the known nonoscillatory behavior along with  $C_2$ ,  $C_3$ , and  $\Phi$ , which are, respectively, the amplitudes and the phase related to the log-periodic oscillatory term. The parameter  $C_3$  is the three-body contact, closely related to the Efimov effect because it gives the amplitude of the log-periodic function of the momentum distribution.

The contact parameter  $C_3$  and the phase  $\Phi$  of the log-periodic asymptotic density, Eq. (3.16), are computed by adding Eqs. (A3), (B7), (C4), and (D4).  $C'_3$  is obtained by adding Eqs. (A4), (B8), (C5), and (D5). Both parameters  $C_3$  and  $C'_3$  scale with  $\kappa_0^2$  or, equivalently, the three-body bound-state energy.

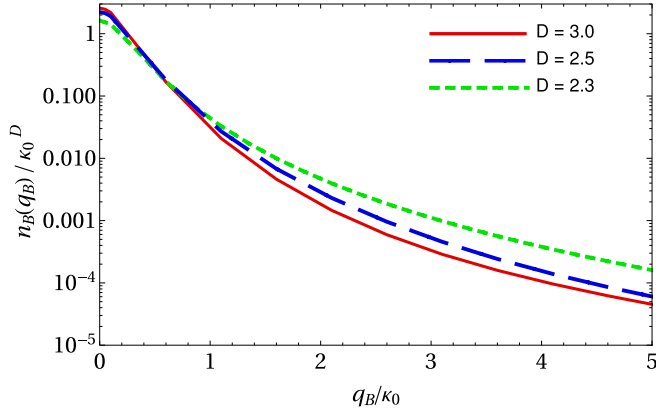


FIG. 2. Single-particle momentum distribution  $n_B(q_B)$  of an  ${}^6\text{Li}-{}^{133}\text{Cs}_2$  Efimov state for  $D = 3$  (solid line),  $D = 2.5$  (long-dashed line), and  $D = 2.3$  (short-dashed line).

#### IV. QUANTITATIVE RESULTS

In this section, we present the numerical results for the momentum density in noninteger dimensions computed from Eq. (3.7) with the exact spectator function (2.16), as well as the subleading contributions to the density given by Eq. (3.16). We provide examples for real systems, and the contact parameters  $C_2$  [from Eq. (3.15)],  $C_3$ , and  $C_3'$  are compared with known results for three dimensions.

##### A. Momentum density

The normalized momentum density  $n_B(q_B)$  is shown for the low-momentum region in Fig. 2, considering the  ${}^6\text{Li}-{}^{133}\text{Cs}_2$  system in 3, 2.5, and 2.3 dimensions. The results for  $D = 2.3$  situate close to the critical dimension where the transition between the regimes of the Efimov discrete-scale symmetry and the continuum one takes place. We observe that by lowering the noninteger dimension, the squeezing of the system tends to emphasize the large-momentum region or short distances; this naively reflects a well-known result in two dimensions: any weakly attractive potential is enough to bind the system for the lowest angular momentum state.

Consequently, the large-momentum region is privileged, which is also expressed by the enhancement of the momentum density and the associated two- and three-body contacts. This becomes evident in Fig. 2 when one follows the decrease of the noninteger dimension by observing that density is depleted close to  $q_B = 0$  and enhanced for larger values of  $q_B/\kappa_0$ . What is visible in Fig. 2 is essentially the tail  $C_2/q_B^4$ , which indicates that  $C_2$  increases considerably from 3 to the critical dimension, where the Efimov effect vanishes.

In Fig. 3, we show the results for the subtracted single-particle momentum distribution  $[n_B(q_B) - C_2/q_B^4]$  for an Efimov state of the  ${}^6\text{Li}-{}^{133}\text{Cs}_2$  system in 3 (top panel), 2.5 (middle panel), and 2.3 (bottom panel) dimensions. The results are obtained from computing Eq. (3.7) with the exact spectator function (2.16). These results are compared with the subleading terms in the asymptotic expansion given in Eq. (3.16), and we find that the asymptotic region is reached quite quickly and the condition  $q_B \gg \kappa_0$  can be relaxed to  $q_B \gtrsim \kappa_0$ .

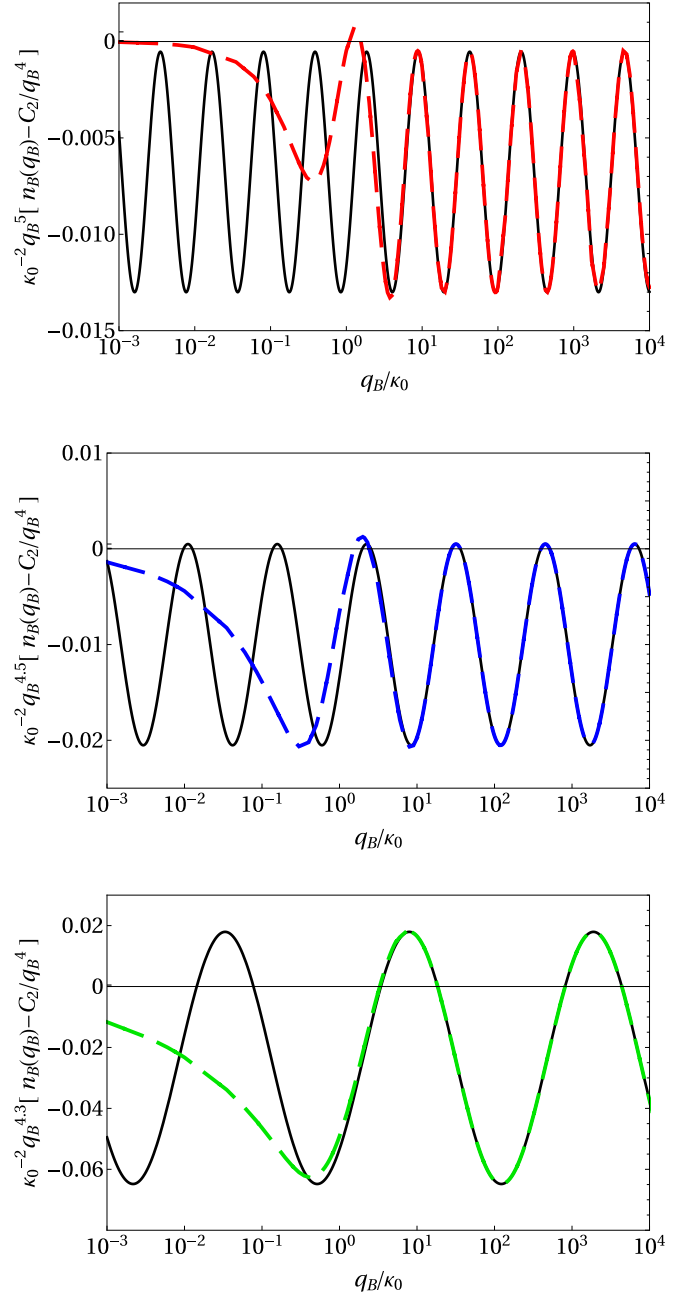


FIG. 3. Subtracted single-particle momentum distribution,  $n_B(q_B) - C_2/q_B^4$ , of an  ${}^6\text{Li}-{}^{133}\text{Cs}_2$  Efimov state for  $D = 3$  (top panel),  $D = 2.5$  (middle panel), and  $D = 2.3$  (bottom panel). Results are obtained with the regular spectator function (2.16) (dashed lines) and subtracted asymptotic formula obtained with Eq. (2.18) (solid lines).

Comparing the top, middle, and bottom panels, we observe the increasing separation between the nodes of the momentum distribution for 3, 2.5, and 2.3 dimensions, tending to infinity as the system approaches the critical dimension, where the Efimov effect disappears. The wavelength associated with the log periodicity at large momentum is directly related to the value of the Efimov parameter for each noninteger dimension, such that it diverges towards the critical dimension where  $s_0 \rightarrow 0$ .

TABLE I. Comparison with the contacts for  $D = 3$  obtained in Refs. [29,49]. The results from Ref. [29] were multiplied by a factor of  $3(2\pi)^3$  to agree with the normalization in Eq. (3.6).

$m_B/m_A$	Contacts	Ref. [49]	Ref. [29]	This work
6/133	$C_2$	0.0274		0.0301
	$C_3$			0.0062
	$C'_3$			-0.0067
	$\Phi$			-4.5201
1	$C_2$	0.0715	0.0713	0.0713
	$C_3$		0.1199	0.1199
	$C'_3$	0	0	0
	$\Phi$		-0.8728	-0.8728

It is also possible to observe in Fig. 3 that the amplitude of the log-periodic oscillations increases with a decrease in the dimension from 3 to 2.3. This effect corresponds to the enhancement of  $C_3$  by lowering the noninteger dimension, mimicked by strengthening the three-dimensional confinement of the system in one direction. Furthermore, we notice that the mean value reflected in  $|C'_3|$  also increases. In what follows, we will further explore the dependence of the contact parameters by changing the noninteger dimension in two systems:  ${}^6\text{Li}$  -  ${}^{133}\text{Cs}_2$  and one with three identical bosons.

### B. Contact parameters

We start by presenting our results for the contacts and phase for three-particle systems in three dimensions. In Table I, we compare our calculations with results from Ref. [49] for  $m_B/m_A = 6/133$  and from Ref. [29] for  $m_B/m_A = 1$ . The small discrepancy between our results for  $C_2$  and the ones from Ref. [49] is due to the choice of the second excited Efimov state in that work, while in the present work we have an arbitrarily high excited state.

Figure 4 illustrates the dependence of  $C_2$ ,  $C_3$ ,  $C'_3$ , and  $\Phi$  on the mass ratio, ranging from heavy-heavy-light to light-light-heavy systems. In the top panel, we show results for the two- and three-body parameters,  $C_2$ ,  $C_3$ , and  $C'_3$ , considering a wide range of mass-imbalanced three-body systems. In the bottom panel of Fig. 4, we show the results for the phase  $\Phi$  of the subleading log-periodic term in the asymptotic form of the momentum density. We observe that  $C_3$ ,  $C'_3$ , and  $\Phi$  saturate for the light-light-heavy system ( $m_B/m_A \gg 1$ ), in addition to  $C_2$ . Furthermore, for  $m_B/m_A \gg 1$ , the heavy particle  $B$  tends to be closer to the center of mass of the  $AAB$  system, increasing the probability of finding it in the large-momentum region, which is reflected in the large values of the contacts. At the other extreme of  $m_B/m_A \ll 1$ , where the Efimov parameter increases and the density of the light particle  $B$  becomes very diffuse, making it less likely to find it at small distances, the contacts decrease.

We should observe that the three-body parameter  $C_3$  is finite for any mass ratio. For three identical bosons, the contact  $C'_3$  vanishes, as already shown in Ref. [29]. In this case, the subleading contribution to the momentum distribution presents a log-periodic oscillation around zero. For all the other cases where  $m_A \neq m_B$ , we found that  $C'_3$  is finite,

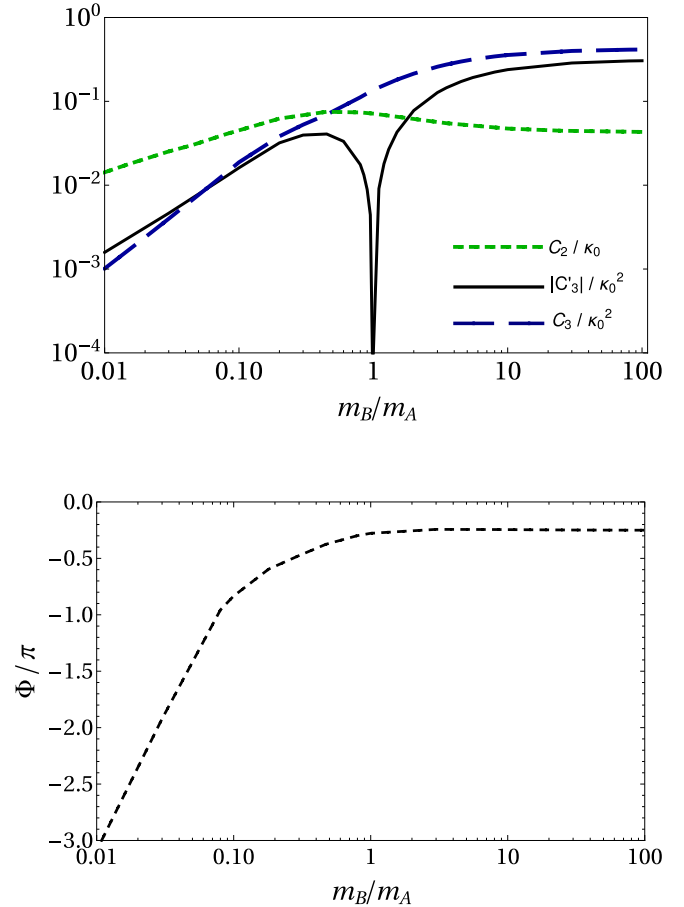


FIG. 4. Three- and two-body contact parameters (top panel) and phase (bottom panel), considering an  $AAB$  system with different mass ratios embedded in three dimensions.

which is in agreement with the results obtained numerically in Ref. [49].

A comment is appropriate here. Reference [31] showed that a universal relation links  $C_3$  to the derivative of the energy with respect to the three-body parameter. We expect that the term proportional to  $C'_3$  will not contribute to this relation since, in the asymptotic momentum density, this contact appears in Eq. (3.16) without explicit dependence on the three-body parameter (represented by  $\kappa_0^*$ ), contrary to  $C_3$ , which comes with the log-periodic dependence on the three-body parameter.

In Fig. 5, we show the dependence of the contacts and phase on the noninteger dimension for the  ${}^6\text{Li}$  -  ${}^{133}\text{Cs}_2$  system from noninteger dimension 2.3 up to 3. In the top panel, we observe that the contacts decrease when moving from 2.3 to 3 dimensions, which can be understood as the system turning out to be more dilute for a fixed binding energy as the dimension increases, and in this particular case,  ${}^6\text{Li}$  is less likely to be found at short distances as one increases the dimension. Therefore, the asymptotic tail for large momentum is depleted by increasing the dimension, which is reflected in the lowering of the contacts. For completeness, we present in the bottom panel the phase as a function of the dimension.

Finally, in Fig. 6, we consider the case of three resonantly interacting identical bosons. We change the noninteger di-

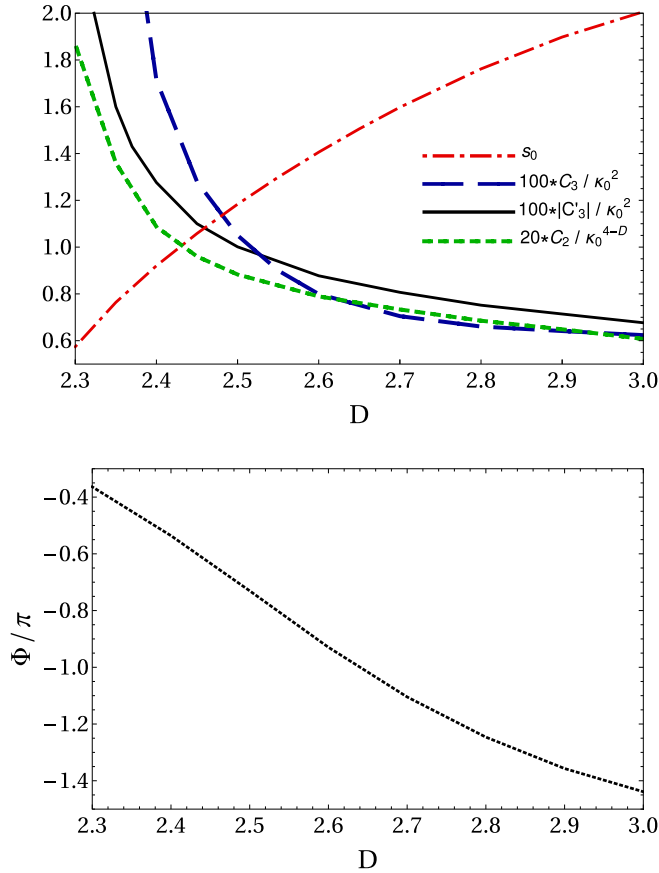


FIG. 5. Three- and two-body contact parameters and phase for the  ${}^6\text{Li}$ - ${}^{133}\text{Cs}_2$  system in noninteger dimensions from 2.3 to 3. Top:  $100 C_3'/\kappa_0^2$  (solid line),  $100 |C_3|/\kappa_0^2$  (long-dashed line),  $20 |C_2|/\kappa_0^{4-D}$  (short-dashed line), and  $s_0$  (dot-dashed line). Bottom: phase  $\Phi/\pi$  (dotted line).

mension from 3 to  $D = 2.4$ . In this case, the Efimov effect is present until the critical dimension of  $D_c = 2.3$ , which corresponds to a squeezed trap with  $b_{ho}/r_{2D} = \sqrt{0.994}$ . We observe in Fig. 6 that  $C_3'$  is always zero, while towards the critical dimension the two- and three-body contacts increase, and the phase approaches a value of  $-0.737$  for  $D = 2.4$  or a squeezed trap with  $b_{ho}/r_{2D} = \sqrt{1.429}$ .

## V. SUMMARY

In this work, we calculated the single-particle momentum distribution of an Efimov mass-imbalanced state in noninteger dimensions at unitarity. We used the wave function of an Efimov state with a finite three-body binding energy, obtained previously in Ref. [43]; in that work, the three-body energy eigenstate was derived in configuration space by considering the Bethe-Peierls boundary conditions in the limit of a zero-range interaction and infinite two-body scattering length.

We studied the single-particle momentum distribution in terms of the relative momentum of particle  $B$  with respect to the  $AA$  subsystem. For that, the Fourier transform of the Efimov state wave function was performed while relying on the spectator functions obtained analytically by the application of the free resolvent to each Faddeev component of the wave

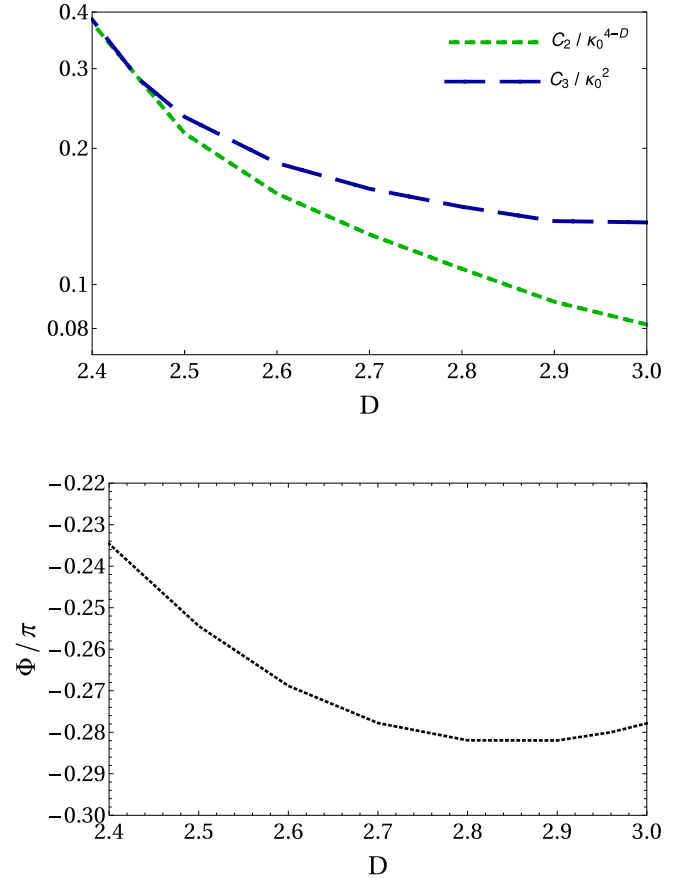


FIG. 6. Three- and two-body contact parameters and phase for three identical bosons in noninteger dimensions. Top:  $C_3/\kappa_0^2$  (long-dashed line) and  $C_2/\kappa_0^{4-D}$  (short-dashed line). Bottom: phase  $\Phi/\pi$  (dotted line).

function, following the method developed in Ref. [29]. These spectator functions depend only on the relative momentum of the spectator particle to the center of mass of the interacting pair. They have characteristic log-periodic oscillations at large momentum, which depend on the noninteger dimension. Furthermore, due to the finite three-body binding energy, the spectator functions are finite for vanishing momentum. Their analytical form reproduces the known numerical results from the literature [49].

The task of deriving the leading and subleading contributions to the high-momentum tail of the single-particle momentum density and the associated two- and three-body contact parameters was made possible by using the analytic form of the spectator functions in momentum space. Independent of the noninteger dimension, the leading nonoscillatory large-momentum tail scales as  $1/q^4$  [see Eqs. (3.14) and (3.16)] and is normalized by the two-body contact. The subleading term is proportional to  $1/q^{D+2}$ ; it is composed of the sum of two contributions, a log-periodic one and a nonoscillatory one, each of which is normalized by the corresponding three-body contact, as shown in Eq. (3.16).

The contact parameters were then computed by decreasing the noninteger dimension starting from three dimensions, where the Efimov discrete scaling drives the physics of the three-body system, to close to the critical dimension, where



the transition to the continuum-scale symmetry takes place. We found that the two- and three-body parameters tend to increase in magnitude close to the critical dimension, independent of the mass imbalance of the three-body system.

We explored in detail the systems formed by  ${}^6\text{Li}$ - ${}^{133}\text{Cs}_2$  and three identical bosons. The parameter  $C'_3$ , normalizing the subleading nonoscillatory term, is zero for three identical bosons regardless of the noninteger dimension. For the  ${}^6\text{Li}$ - ${}^{133}\text{Cs}_2$  system, we found that the two- and three-body contact parameters increase close to the critical dimension where the Efimov effect disappears. Furthermore, in this case, the phase of the log-periodic term approaches  $-1.143$  for  $D = 2.4$ . The expectation of the growth of the two- and three-body contact parameters with the decrease of the noninteger dimension seems natural, as one can naively infer that, in this situation, the particles have the chance to stay closer to the system confined in an oblate trap.

In summary, we have explored different aspects of the momentum density of particle  $B$  for mass-imbalanced  $AAB$  systems in noninteger dimensions, which can be a useful probe of the effect of trap deformation on few-body dynamics and on the Efimov phenomenon. The hallmark of this transition from three dimensions to the critical dimension where the Efimov effect vanishes can be seen in the asymptotic momentum distribution, where we showed that the contact parameters grow and, consequently, so do their effects on the evolution of the many-body properties with the decrease of the noninteger dimension.

#### ACKNOWLEDGMENTS

This work was partially supported by Fundação de Amparo à Pesquisa do Estado de São Paulo [FAPESP; Grants No. 2017/05660-0 and No. 2019/07767-1 (T.F.), No. 2020/00560-0 (D.S.R.), and No. 2018/25225-9 (G.K.)] and Conselho Nacional de Desenvolvimento Científico e Tecnológico [CNPq; Grants No. 308486/2015-3 (T.F.), No. 303579/2019-6 (M.T.Y.), and No. 309262/2019-4 (G.K.)].

#### APPENDIX A: SUBLEADING CONTRIBUTIONS TO $n_1(q_B)$

Equation (3.8) can be written in spherical coordinates as

$$n_1(q_B) = |\chi^{(B)}(q_B)|^2 \mathcal{S}_D \int_0^\infty dp_B \frac{p_B^{D-1}}{(E_3 + p_B^2 + \frac{q_B^2}{2\mu_B})^2}, \quad (\text{A1})$$

where  $\mathcal{S}_D = 2\pi^{D/2}/\Gamma(D/2)$ . Changing variables  $p_B/q_B = p'_B$  and considering  $q_B \gg \sqrt{2\mu_B E_3}$  allow us to write

$$\begin{aligned} n_1(q_B) &= \frac{|\chi^{(B)}(q_B)|^2}{q_B^{4-D}} \mathcal{S}_D \int_0^\infty dp'_B \frac{p'^{D-1}_B}{(p'^2_B + 1/2\mu_B)^2} \\ &= \frac{|\chi^{(B)}(q_B)|^2}{q_B^{4-D}} \mathcal{S}_D \frac{(2-D)\pi}{4} \csc\left(\frac{D\pi}{2}\right) (2\mu_B)^{2-D/2}. \end{aligned} \quad (\text{A2})$$

For large momentum, we use the asymptotic spectral function, Eq. (2.18), and from simple manipulations we separate the oscillatory term, namely, the log-periodic one,

$$\begin{aligned} n_1^{\text{osc}}(q_B) &= \frac{|C^{(B)}|^2}{q_B^{D+2}} \cos\left[2s_0 \ln\left(\frac{q_B}{\sqrt{2\mu_B \kappa_0^*}}\right)\right] |\mathfrak{F}_{(D,s_0)}|^2 \\ &\quad \times \mathcal{S}_D \pi \left(1 - \frac{D}{2}\right) [\text{Re}(\mathcal{G})^2 + \text{Im}(\mathcal{G})^2] \\ &\quad \times (2\mu_B)^{1+D/2} \csc\left(\frac{D\pi}{2}\right), \end{aligned} \quad (\text{A3})$$

and the nonoscillatory part,

$$\begin{aligned} n_1^{\text{nosc}}(q_B) &= \frac{|C^{(B)}|^2}{q_B^{D+2}} |\mathfrak{F}_{(D,s_0)}|^2 \mathcal{S}_D \pi \left(1 - \frac{D}{2}\right) (2\mu_B)^{1+D/2} \\ &\quad \times [\text{Re}(\mathcal{G})^2 + \text{Im}(\mathcal{G})^2] \csc\left(\frac{D\pi}{2}\right), \end{aligned} \quad (\text{A4})$$

where  $\mathcal{G}$  is written in Eq. (2.19).

#### APPENDIX B: SUBLEADING CONTRIBUTIONS TO $n_2(q_B)$

Taking the large-momentum limit, where  $q_B \gg \sqrt{2\mu_B E_3}$ , and changing the variables to  $\mathbf{q}_A = \mathbf{p}_B - \mathbf{q}_B/2$ , Eq. (3.9) can be written as

$$n_2(q_B) = 2 \int d^D q_A \frac{|\chi^{(A)}(q_A)|^2}{(q_A^2 + \mathbf{q}_A \cdot \mathbf{q}_B + q_B^2/2\mu_B)^2}. \quad (\text{B1})$$

In spherical coordinates we have

$$n_2(q_B) = \frac{2(2\pi)^{D-3}}{q_B^4} \prod_{k=1}^{D-3} \int_0^\pi d\theta_k \sin^k \theta_k \int_0^\infty dq_A q_A^{D-1} |\chi^{(A)}(q_A)|^2 \int_0^\pi d\theta \sin^{D-2} \theta \frac{1}{[(q_A/q_B)^2 + (q_A/q_B) \cos \theta + (\mathcal{A} + 1)/2\mathcal{A}]^2}; \quad (\text{B2})$$

changing the variables to  $q'_A = q_A/q_B$ , we find that

$$n_2(q_B) = \frac{2\mathcal{S}_D}{q_B^{4-D}} \int_0^\infty dq'_A q'^{D-1}_A |\chi^{(A)}(q_B q'_A)|^2 \mathcal{H}(q'_A), \quad (\text{B3})$$

with

$$\mathcal{H}(y) = \frac{4\mathcal{A}^2(D-2)}{\mathcal{A}^2(4y^4+1) + \mathcal{A}(4y^2+2) + 1} + \frac{4\mathcal{A}^2(3-D)(2y^2\mathcal{A} + \mathcal{A} + 1)}{[2\mathcal{A}(y-1)y + \mathcal{A} + 1]^2[2y(y+1)\mathcal{A} + \mathcal{A} + 1]} \\ \times H_2F_1\left(1, \frac{D-1}{2}, D-1, -\frac{4\mathcal{A}y}{2(y-1)y\mathcal{A} + \mathcal{A} + 1}\right), \quad (\text{B4})$$

where  $H_2F_1(a, b, c, z)$  is the hypergeometrical function.

In order to separate the oscillatory and nonoscillatory contributions in  $n_2(q_B)$  (B3), we perform the following manipulation:

$$n_2(q_B) = \frac{2S_D}{q_B^{4-D}} \int_0^\infty dq'_A q_A^{D-1} |\chi^{(A)}(q_B q'_A)|^2 \left( \mathcal{H}(q'_A) - \frac{4\mathcal{A}^2}{(\mathcal{A}+1)^2} \right) + \frac{C_2}{q_B^4}, \quad (\text{B5})$$

where  $C_2$  is the two-body contact parameter and was written in Eq. (3.15).

In order to derive the oscillatory part of  $n_2(q_B)$  at large momentum, we introduce the asymptotic spectator function, Eq. (2.18), in the first term of Eq. (B5), i.e.,  $n_2(q_B) - C_2/q_B^4 \cdot \cos^2$  from the asymptotic expression for  $|\chi^{(A)}(q_B q'_A)|^2$  is algebraically manipulated in the form

$$\cos^2 \left[ s_0 \ln \left( \frac{q'_A q_B}{\sqrt{2\mu_A \kappa_0^*}} \right) \right] = \frac{1}{2} + \frac{1}{2} \left\{ \cos \left[ 2s_0 \ln \left( \frac{q_B}{\sqrt{2\mu_A \kappa_0^*}} \right) \right] \cos[2s_0 \ln(q'_A)] \right. \\ \left. - \sin \left[ 2s_0 \ln \left( \frac{q_B}{\sqrt{2\mu_A \kappa_0^*}} \right) \right] \sin[2s_0 \ln(q'_A)] \right\}. \quad (\text{B6})$$

We can write the oscillatory term as

$$n_2^{\text{osc}}(q_B) - \frac{C_2}{q_B^4} = \frac{|C^{(A)}|^2}{q_B^{D+2}} \frac{2^{1+D} S_D}{\mu_A^{1-D}} [\text{Re}(\mathcal{G})^2 + \text{Im}(\mathcal{G})^2] |\mathfrak{F}_{(D,s_0)}|^2 \int_0^\infty dq'_A q_A^{1-D} \left( \mathcal{H}(q'_A) - \frac{4\mathcal{A}^2}{(\mathcal{A}+1)^2} \right) \\ \times \left\{ \cos \left[ 2s_0 \ln \left( \frac{q_B}{\sqrt{2\mu_A \kappa_0^*}} \right) \right] \cos[2s_0 \ln(q'_A)] - \sin \left[ 2s_0 \ln \left( \frac{q_B}{\sqrt{2\mu_A \kappa_0^*}} \right) \right] \sin[2s_0 \ln(q'_A)] \right\} \quad (\text{B7})$$

and the nonoscillatory one as

$$n_2^{\text{nos}}(q_B) - \frac{C_2}{q_B^4} = \frac{|C^{(A)}|^2}{q_B^{D+2}} \frac{2^{1+D} S_D}{\mu_A^{1-D}} [\text{Re}(\mathcal{G})^2 + \text{Im}(\mathcal{G})^2] |\mathfrak{F}_{(D,s_0)}|^2 \int_0^\infty dq'_A q_A^{1-D} \left( \mathcal{H}(q'_A) - \frac{4\mathcal{A}^2}{(\mathcal{A}+1)^2} \right). \quad (\text{B8})$$

### APPENDIX C: SUBLEADING CONTRIBUTIONS TO $n_3(q_B)$

Taking  $n_3(q_B)$  from Eq. (3.10) with the change in variables  $\mathbf{p}_B - \mathbf{q}_B/2 = \mathbf{q}_A$  and considering the large-momentum limit, namely,  $q_B \gg \sqrt{2\mathcal{A}E_3}/(\mathcal{A}+1)$ , we can write

$$n_3(q_B) = \int d^D q_A \frac{2\chi^{(B)*}(q_B) \chi^{(A)}(q_A)}{(q_A^2 + \mathbf{q}_A \cdot \mathbf{q}_B + q_B^2 \frac{\mathcal{A}+1}{2\mathcal{A}})^2} + \text{c.c.} \quad (\text{C1})$$

The spectator functions are real; once again, after changing the variables  $q_A/q_B = q'_A$  and integrating in spherical coordinates, we get

$$n_3(q_B) = \chi^{(B)*}(q_B) \frac{4S_D}{q_B^{4-D}} \int_0^\infty dq'_A q_A^{D-1} \chi^{(A)}(q_B q'_A) \mathcal{H}(q'_A), \quad (\text{C2})$$

where  $\mathcal{H}(q'_A)$  is given by Eq. (B4). The asymptotic form is found by using the spectator function from Eq. (2.18), leading to

$$n_3(q_B) = \frac{C^{(B)*} C^{(A)}}{q_B^{D+2}} 2^{D+3} S_D (\mu_B \mu_A)^{D/2-1/2} [\text{Re}(\mathcal{G})^2 + \text{Im}(\mathcal{G})^2] \left\{ \cos \left[ s_0 \ln \left( \frac{q_B}{\sqrt{2\mu_B \kappa_0^*}} \right) \right] \right. \\ \times \cos \left[ s_0 \ln \left( \frac{q_B}{\sqrt{2\mu_A \kappa_0^*}} \right) \right] \int_0^\infty dq'_A \mathcal{H}(q'_A) \cos[s_0 \ln(q'_A)] \\ \left. - \sin \left[ s_0 \ln \left( \frac{q_B}{\sqrt{2\mu_B \kappa_0^*}} \right) \right] \sin \left[ s_0 \ln \left( \frac{q_B}{\sqrt{2\mu_A \kappa_0^*}} \right) \right] \int_0^\infty dq'_A \mathcal{H}(q'_A) \sin[s_0 \ln(q'_A)] \right\}. \quad (\text{C3})$$

The algebraic manipulation of the cosines and sines in the equation above allows us to identify the oscillatory term as

$$n_3^{\text{osc}}(q_B) = \frac{C^{(B)*} C^{(A)}}{q_B^{D+2}} 2^{D+2} S_D(\mu_B \mu_A)^{D/2-1/2} |\mathfrak{F}_{(D,s_0)}|^2 [\text{Re}(\mathcal{G})^2 + \text{Im}(\mathcal{G})^2] \left\{ \cos \left[ s_0 \ln \left( \frac{q_B^2 / \kappa_0^{*2}}{2\sqrt{\mu_A \mu_B}} \right) \right] \right. \\ \left. \times \int_0^\infty dq'_A \mathcal{H}(q'_A) \cos[s_0 \ln(q'_A)] - \sin \left[ s_0 \ln \left( \frac{q_B^2 / \kappa_0^{*2}}{2\sqrt{\mu_A \mu_B}} \right) \right] \int_0^\infty dq'_A \mathcal{H}(q'_A) \sin[s_0 \ln(q'_A)] \right\} \quad (\text{C4})$$

and the nonoscillatory one as

$$n_3^{\text{nossc}}(q_B) = \frac{C^{(B)*} C^{(A)}}{q_B^{D+2}} 2^{D+2} S_D(\mu_B \mu_A)^{D/2-1/2} |\mathfrak{F}_{(D,s_0)}|^2 [\text{Re}(\mathcal{G})^2 + \text{Im}(\mathcal{G})^2] \left\{ \cos \left[ s_0 \ln \left( \sqrt{\frac{\mu_B}{\mu_A}} \right) \right] \right. \\ \left. \times \int_0^\infty dq'_A \mathcal{H}(q'_A) \cos[s_0 \ln(q'_A)] - \sin \left[ s_0 \ln \left( \sqrt{\frac{\mu_B}{\mu_A}} \right) \right] \int_0^\infty dq'_A \mathcal{H}(q'_A) \sin[s_0 \ln(q'_A)] \right\}. \quad (\text{C5})$$

#### APPENDIX D: SUBLEADING CONTRIBUTIONS TO $n_4(q_B)$

The argument of the spectator function in Eq. (3.11) is

$$\left| \mathbf{p}_B \pm \frac{\mathbf{q}_B}{2} \right| = q_B \sqrt{\frac{p_B^2}{q_B^2} + \frac{1}{4} \pm \frac{p_B}{q_B} \cos \theta}; \quad (\text{D1})$$

then changing the variables to  $p_B/q_B = p'_B$  and considering the large-momentum limit, we have

$$n_4(q_B) = \frac{1}{q_B^{4-D}} 4\pi \prod_{k=1}^{D-3} \int_0^\pi d\theta_k \sin^k(\theta_k) \int_0^\infty dp'_B \frac{p_B'^{D-1}}{[p_B'^2 + (\mathcal{A} + 2)/4\mathcal{A}]^2} \int_0^\pi d\theta \sin^{D-2} \theta \chi^{(A)*}(q_B p'_{B-}) \chi^{(A)}(q_B p'_{B+}), \quad (\text{D2})$$

where  $p'_{B\pm} = \sqrt{p_B'^2 + \frac{1}{4} \pm p'_B \cos \theta}$ . The product of the spectator functions (2.18) allow us to write

$$\chi^{(A)*}(q_B p'_{B-}) \chi^{(A)}(q_B p'_{B+}) = |C^{(A)}|^2 [\text{Re}(\mathcal{G})^2 + \text{Im}(\mathcal{G})^2] 2 |\mathfrak{F}_{(D,s_0)}|^2 \left( \frac{q_B}{\sqrt{2\mu_A}} \sqrt{p'_{B-} p'_{B+}} \right)^{2-2D} \\ \times \left\{ \cos \left[ s_0 \ln \left( \frac{p'_{B+}}{p'_{B-}} \right) \right] + \cos \left[ s_0 \ln \left( \frac{q_B^2 p'_{B+} p'_{B-}}{2\mu_A \kappa_0^{*2}} \right) \right] \right\}. \quad (\text{D3})$$

Then, the oscillatory contribution in Eq. (D2) is

$$n_4^{\text{osc}}(q_B) = \frac{|C^{(A)}|^2 2^{2+D} \pi^{D/2-1/2}}{q_B^{D+2} \Gamma[D/2 - 1/2]} |\mathfrak{F}_{(D,s_0)}|^2 \mu_A^{D-1} [\text{Re}(\mathcal{G})^2 + \text{Im}(\mathcal{G})^2] \\ \times \int_0^\infty dp'_B \frac{p_B'^{D-1}}{[p_B'^2 + (\mathcal{A} + 2)/4\mathcal{A}]^2} \int_0^\pi d\theta \sin^{D-2} \theta \mathcal{W}^{1/2-D/2} \cos \left[ s_0 \ln \left( \frac{q_B^2}{2\mu_A \kappa_0^{*2}} \mathcal{W}^{1/2} \right) \right], \quad (\text{D4})$$

where

$$\mathcal{W} = (p_B'^2 + \frac{1}{4} + p'_B \cos \theta)(p_B'^2 + \frac{1}{4} - p'_B \cos \theta).$$

The nonoscillatory contribution in Eq. (D2) can be identified as

$$n_4^{\text{nossc}}(q_B) = \frac{|C^{(A)}|^2 2^{2+D} \pi^{D/2-1/2}}{q_B^{D+2} \Gamma[D/2 - 1/2]} |\mathfrak{F}_{(D,s_0)}|^2 \mu_A^{D-1} [\text{Re}(\mathcal{G})^2 + \text{Im}(\mathcal{G})^2] \int_0^\infty dp'_B \frac{p_B'^{D-1}}{[p_B'^2 + (\mathcal{A} + 2)/4\mathcal{A}]^2} \\ \times \int_0^\pi d\theta \sin^{D-2} \theta \mathcal{W}^{1/2-D/2} \cos \left[ s_0 \ln \left( \sqrt{\frac{p_B'^2 + \frac{1}{4} + p'_B \cos \theta}{p_B'^2 + \frac{1}{4} - p'_B \cos \theta}} \right) \right]. \quad (\text{D5})$$

#### APPENDIX E: CONTACT PARAMETERS AND PHASES FOR MASS-IMBALANCED SYSTEMS

Table II displays numerical results for the two- and three-body contact parameters and phases for several mass-imbalanced atomic systems for  $D = 3$ . We also show the mass ratio and Efimov scale parameter for each weakly bound molecule. Our findings are in agreement with those from Ref. [49] for  $m_B/m_A = 6/133$  and from Ref. [29] for  $m_B/m_A = 1$ .

TABLE II. Two- and three-body contact parameters and phases for several mass-imbalanced systems for  $D = 3$ .

System	$m_B/m_A$	$C_2/\kappa_0$	$C_3/\kappa_0^2$	$C'_3/\kappa_0^2$	$\Phi$	$s_0$
$^{174}\text{Yb}_2 - ^6\text{Li}$	0.0345	0.0277	0.0049	-0.0056	-5.5376	2.2590
$^{133}\text{Cs}_2 - ^6\text{Li}$	0.0451	0.0301	0.0062	-0.0067	-4.5201	2.0059
$^{87}\text{Rb}_2 - ^6\text{Li}$	0.0690	0.0387	0.0120	-0.0113	-3.4030	1.6833
$^{41}\text{K}_2 - ^6\text{Li}$	0.1463	0.0551	0.0289	-0.0239	-2.0926	1.3019
$^{23}\text{Na}_2 - ^6\text{Li}$	0.2609	0.0679	0.0497	-0.0379	-1.5428	1.1331
$^{87}\text{Rb}_2 - ^{41}\text{K}$	0.4713	0.0754	0.0770	-0.0395	-1.1413	1.0406
$^{133}\text{Cs}_2 - ^{87}\text{Rb}$	0.6544	0.0753	0.0968	-0.0271	-0.9814	1.0162
$^{133}\text{Cs}_3$	1.0000	0.0713	0.1199	0.0000	-0.8728	1.0062
$^{41}\text{K}_2 - ^{87}\text{Rb}$	2.1219	0.0625	0.2229	0.0872	-0.7819	1.0269

- [1] M. Zaccanti, B. Deissler, C. D'Errico, M. Fattori, M. Jonas-Lasinio, S. Müller, G. Roati, M. Inguscio, and G. Modugno, *Nature Phys.* **5**, 586 (2009).
- [2] S. Knoop, F. Ferlaino, M. Mark, M. Berninger, H. Schöbel, H.-C. Nägerl, and R. Grimm, *Nat. Phys.* **5**, 227 (2009).
- [3] J. R. Williams, E. L. Hazlett, J. H. Huckans, R. W. Stites, Y. Zhang, and K. M. O'Hara, *Phys. Rev. Lett.* **103**, 130404 (2009).
- [4] R. Pires, J. Ulmanis, S. Häfner, M. Repp, A. Arias, E. D. Kuhnle, and M. Weidemüller, *Phys. Rev. Lett.* **112**, 250404 (2014).
- [5] S.-K. Tung, K. Jiménez-García, J. Johansen, C. V. Parker, and C. Chin, *Phys. Rev. Lett.* **113**, 240402 (2014).
- [6] R. S. Bloom, M.-G. Hu, T. D. Cumby, and D. S. Jin, *Phys. Rev. Lett.* **111**, 105301 (2013).
- [7] C. Chin, R. Grimm, P. Julienne, and E. Tiesinga, *Rev. Mod. Phys.* **82**, 1225 (2010).
- [8] A. J. Leggett, *Rev. Mod. Phys.* **73**, 307 (2001); **75**, 1083 (2003).
- [9] D. S. Petrov, M. Holzmann, and G. V. Shlyapnikov, *Phys. Rev. Lett.* **84**, 2551 (2000).
- [10] M. Greiner, I. Bloch, O. Mandel, T. W. Hänsch, and T. Esslinger, *Appl. Phys. B* **73**, 769 (2001).
- [11] V. Efimov, *Phys. Lett. B* **33**, 563 (1970).
- [12] V. N. Efimov, *Sov. J. Nucl. Phys.* **12**, 589 (1971).
- [13] E. Braaten and H.-W. Hammer, *Phys. Rep.* **428**, 259 (2006).
- [14] P. Naidon and S. Endo, *Rep. Prog. Phys.* **80**, 056001 (2017).
- [15] C. H. Greene, P. Giannakeas, and J. Perez-Rios, *Rev. Mod. Phys.* **89**, 035006 (2017).
- [16] H. W. Hammer, S. König, and U. van Kolck, *Rev. Mod. Phys.* **92**, 025004 (2020).
- [17] T. Kraemer, M. Mark, P. Waldburger, J. G. Danzl, C. Chin, B. Engeser, A. D. Lange, K. Pilch, A. Jaakkola, H.-C. Nägerl, and R. Grimm, *Nature (London)* **440**, 315 (2006).
- [18] R. J. Fletcher, A. L. Gaunt, N. Navon, R. P. Smith, and Z. Hadzibabic, *Phys. Rev. Lett.* **111**, 125303 (2013).
- [19] S. Musolino, H. Kurkjian, M. Van Regemortel, M. Wouters, S. J. J. M. F. Kokkelmans, and V. E. Colussi, *Phys. Rev. Lett.* **128**, 020401 (2022).
- [20] E. D. Kuhnle, H. Hu, X.-J. Liu, P. Dyke, M. Mark, P. D. Drummond, P. Hannaford, and C. J. Vale, *Phys. Rev. Lett.* **105**, 070402 (2010).
- [21] P. Makotyn, C. Klauss, D. Goldberger, E. Cornell, and D. Jin, *Nat. Phys.* **10**, 116 (2014).
- [22] R. Fletcher, R. Lopes, N. Navon, R. Smith, M. Zwierlein, and Z. Hadzibabic, *Science* **355**, 377 (2017).
- [23] Z. Z. Yan, Y. Ni, C. Robens, and M. W. Zwierlein, *Science* **368**, 190 (2020).
- [24] Y.-Q. Zou, B. Bakkali-Hassani, C. Maury, É. Le Cerf, S. Nascimbene, J. Dalibard, and J. Beugnon, *Nat. Commun.* **12**, 760 (2021).
- [25] S. Tan, *Ann. Phys. (NY)* **323**, 2952 (2008).
- [26] S. Tan, *Ann. Phys. (NY)* **323**, 2971 (2008).
- [27] S. Tan, *Ann. Phys. (NY)* **323**, 2987 (2008).
- [28] E. Braaten, D. Kang, and L. Platter, *Phys. Rev. Lett.* **106**, 153005 (2011).
- [29] Y. Castin and F. Werner, *Phys. Rev. A* **83**, 063614 (2011).
- [30] F. Werner and Y. Castin, *Phys. Rev. A* **86**, 053633 (2012).
- [31] D. H. Smith, E. Braaten, D. Kang, and L. Platter, *Phys. Rev. Lett.* **112**, 110402 (2014).
- [32] T. K. Lim and P. A. Maurone, *Phys. Rev. B* **22**, 1467 (1980).
- [33] T. K. Lim and B. Shimer, *Z. Phys. A* **297**, 185 (1980).
- [34] S. K. Adhikari, A. Delfino, T. Frederico, I. D. Goldman, and L. Tomio, *Phys. Rev. A* **37**, 3666 (1988).
- [35] F. F. Bellotti and M. T. Yamashita, *Few-Body Syst.* **56**, 905 (2015).
- [36] E. Garrido, A. S. Jensen, and R. Álvarez-Rodríguez, *Phys. Lett. A* **383**, 2021 (2019).
- [37] D. S. Rosa, T. Frederico, G. Krein, and M. T. Yamashita, *Phys. Rev. A* **97**, 050701(R) (2018); **104**, 029901 (2021).
- [38] R. M. Francisco, D. S. Rosa, and T. Frederico, *Phys. Rev. A* **106**, 063305 (2022).
- [39] D. S. Rosa, T. Frederico, G. Krein, and M. T. Yamashita, *J. Phys. B* **52**, 025101 (2019).
- [40] E. Garrido and A. S. Jensen, *Phys. Lett. A* **385**, 126982 (2021).
- [41] E. Garrido and A. S. Jensen, *Phys. Rev. Res.* **2**, 033261 (2020).
- [42] E. Nielsen, D. V. Fedorov, A. S. Jensen, and E. Garrido, *Phys. Rep.* **347**, 373 (2001).
- [43] D. S. Rosa, T. Frederico, G. Krein, and M. T. Yamashita, *Phys. Rev. A* **106**, 023311 (2022).
- [44] H. Bethe and R. Peierls, *Proc. R. Soc. Lond. A* **148**, 146 (1935).
- [45] A. Bulgac and V. Efimov, *Sov. J. Nucl. Phys.* **22**, 296 (1975).
- [46] V. Efimov, *Nucl. Phys. A* **210**, 157 (1973).
- [47] W. Magnus, F. Oberhettinger, and R. P. Soni, *Formulas and Theorems for the Special Functions of Mathematical Physics* (Springer, New York, 1966).
- [48] L. H. Thomas, *Phys. Rev.* **47**, 903 (1935).
- [49] M. T. Yamashita, F. F. Bellotti, T. Frederico, D. V. Fedorov, A. S. Jensen, and N. T. Zinner, *Phys. Rev. A* **87**, 062702 (2013).
- [50] F. Werner, *Phys. Rev. A* **78**, 025601 (2008).